



PERGAMON

Quaternary Science Reviews 23 (2004) 175–191



Optically stimulated luminescence dating of Late Quaternary glaciogenic sediments in the upper Hunza valley: validating the timing of glaciation and assessing dating methods

Joel Q. Spencer*, Lewis A. Owen

Department of Earth Sciences, University of California, Riverside, CA 92521-0423, USA

Received 18 August 2002; accepted 14 July 2003

Abstract

We present a comprehensive comparison of optically stimulated luminescence (OSL) ages with cosmogenic radionuclide (CRN) ages, and the first study to validate CRN dates from boulders on moraine ridges using luminescence dates from glaciogenic sediments from associated moraines, accomplished from both direct and stratigraphic relationships between CRN and OSL sampling sites. Both quartz and K-feldspars extracted from 12 Late Quaternary glaciogenic sediments were studied using single-aliquot OSL techniques. Rapid signal saturation in preliminary additive-dose infrared-stimulated K-feldspar luminescence growth data was interpreted as evidence of insufficiently bleached latent luminescence, and these data gave rise to overestimated ages in the majority of samples. Further analysis concentrated on replicated single-aliquot regenerative-dose (SAR) measurements of quartz minerals using blue-green stimulation. The SAR sensitivity correction method repeatedly failed in two of the samples and a further sample exhibited significant thermal transfer. Nevertheless, three of the eight glacial successions in the upper Hunza valley were defined using quartz-luminescence. Although we discuss the possibility of inherited components in the CRN data, in terms of paleoclimatic interpretations both dating techniques give concordant results.

© 2003 Elsevier Ltd. All rights reserved.

1. Introduction

The mountains of the Himalaya and Transhimalaya contain the greatest concentration of glaciers outside of the Polar Regions, constituting about 50% of the total extra-Polar glaciated area (von Wissman, 1959). The Himalayan regions contain impressive successions of moraines that record multiple glaciations, which in turn provide evidence for climatic change during the Late Quaternary (Owen et al., 1998). Unfortunately, few of these glacial successions have been numerically dated. This is mainly because of the scarcity of organic material in these high-energy glaciogenic deposits that is required for standard radiocarbon dating. In recent years, however, optically stimulated luminescence (OSL) and cosmogenic radionuclide (CRN) exposure dating has enabled the direct dating of glacial sediments and

landforms (e.g. Phillips et al., 2000; Richards et al., 2000a, b; Owen et al., 2001, 2002a). Both techniques, however, have problems that are inherent to the methods themselves and/or are related to site-specific factors (Richards, 2000; Owen et al., 2001, 2002a). The vast majority of numerical dating studies in individual study regions within the Himalaya only apply one of these dating techniques. Validation of CRN dating using OSL, with samples from both directly related and stratigraphically related sampling sites, has previously not been attempted. Conversely, Finkel et al. (2003) have successfully tested OSL dates from moraines in the Khumbu Himal using CRN methods.

In this paper, we apply OSL techniques to date a well-defined glacial succession in the Hunza valley, Karakoram Mountains (Fig. 1) that has recently been dated using CRN techniques (Owen et al., 2002a and Table 1). This will help test the established glacial chronology and it will compare OSL and CRN methods. Furthermore, this study will examine the applicability, benefits and problems associated with applying OSL methods to date glaciogenic sediments. The glacial sediments and

*Corresponding author. Present address: School of Geography and Geosciences, University of St. Andrews, Fife, KY16 9AL, Scotland. Tel.: +44-1334-463992; fax: +44-1334-463949.

E-mail address: joel.spencer@st-andrews.ac.uk (J.Q. Spencer).

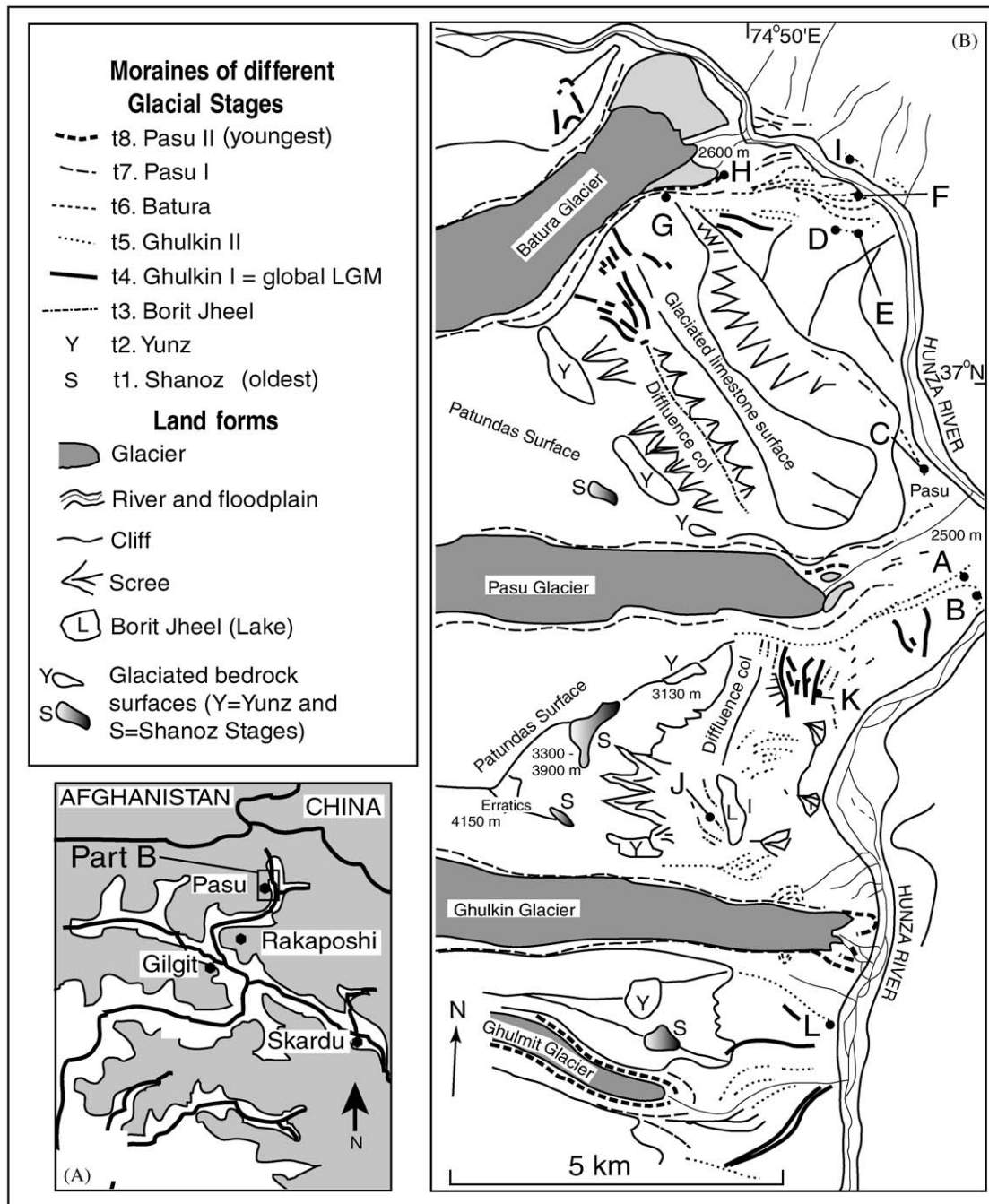


Fig. 1. (A) Location map of the study area and (B) geomorphic map adapted from Derbyshire et al. (1984) showing the main moraines and the sampling sites for OSL dating.

landforms in the Hunza valley, Karakoram Mountains are exceptionally well preserved and they provide evidence for at least eight glacial advances. Derbyshire et al. (1984) provide a sound morphostratigraphy that has been partially defined by four thermoluminescence (TL) and two radiocarbon dates (Table 1 and Fig. 1). This chronology was re-examined by Owen et al. (2002a) who undertook a program of CRN dating that defined the timing of the last five glacial advances to the Last Glacial and Holocene (Table 1). We used this morpho-

stratigraphic and geochronological framework to collect sediment samples for OSL dating.

2. Sampling sites

Twelve locations (A–L in Fig. 1) were examined to collect sediment samples for OSL dating from different geomorphic and sedimentological settings of various ages (Figs. 2 and 3). The 12 sampling locations were related to

Table 1

Quaternary glacial stages in the upper Hunza valley after Derbyshire et al. (1984), showing all the dates presented in their work compared with the range of CRN dates (in bold) from Owen et al. (2002a)

Till unit	Stage name	Tentative date (ka) ^a	Description of the glaciations and the main glacial-geologic evidence
t8	Pasu II	Historical (19th and 20th centuries)	A minor advance of a few hundred metres—sharp-crested, unstable, and sometimes ice-cored moraines with fresh boulders that have no rock varnish
t7	Pasu I	0.83 ± 0.08 ^b 0.325 ± 0.06 ^b	A minor advance of ~1 km, restricted to tributary valleys—high sharp-crested moraines with boulders that have a light yellow surface colour
t6	Batura	No dates ^c ~ 9.0–10.8	A glacial advance of 1–2 km—well defined moraines with strong varnished and weathered boulders
t5	Ghulkin II	No dates ~ 15.3–18.4	Minor glacier advance of several kilometres—a series of rounded moraine ridges with deeply weathered boulders having a strong to postmaximal rock varnish, and a weak carbonate development beneath boulders
t4	Ghulkin I	47.0 ± 2.35 ^d ~ 21.8–25.7	Minor valley glaciation, expanding into diffuence cols and into the main Hunza valley—well-defined moraines with deeply weathered (cavernous) boulders having very strong to postmaximal rock varnish, and incipient calcrete and pendant growth of carbonate
t3	Borit Jheel	65.0 ± 3.3 ^e 50.0 ± 2.5 ^f ~ 43.2–54.7	Main valley glaciations with tributary valley glaciers filling and locally overtopping diffuence cols—highly eroded moraines with deeply weathered boulders having a very strong to postmaximal shiny-black rock varnish, and an extensive underlying calcrete
t2	Yunz	139.0 ± 12.5 ^g > 60	Extensive main valley glaciation—deeply weathered till remnants on benches in the main Hunza valley at an altitude of ~3900 m asl on the upper western slopes of the Pasu–Ghulkin diffuence col
t1	Shanoz	No dates	Extensive broad valley glaciation—deeply weathered erratics on summit surfaces at an altitude of > 4150 m asl

^aFigures in regular font style from Derbyshire et al. (1984). Figures in bold font style are the range of CRN dates from Owen et al. (2002a). No details of the laboratory procedures used to obtain the dates in China were divulged and so could not be reported in Derbyshire et al. (1984).

^bUncalibrated radiocarbon dates on timber from a moraine of the Minapin Glacier, middle Hunza valley.

^cDerbyshire et al. (1984) considered this glacial stage to be middle Holocene in age.

^dTL date on lacustrine silts intercalated with Ghulkin I till of moraines from the Pisan Glacier in the middle Hunza valley.

^eTL date on glaciolacustrine sediments, which were probably deposited during the Borit Jheel Stage, ~1.5 km north of the present snout of the Pasu Glacier.

^fTL date on glaciotectonized glaciolacustrine sediments within Borit Jheel till ~2.5 km south of the snout of the Batura Glacier.

^gTL date on glaciolacustrine silts beneath Borit Jheel till southeast of the Ghulkin I and II Glaciers.

CRN sampling sites (Owen et al., 2002a) on the basis of morphostratigraphy, to enable comparison of OSL ages of sediments within moraines with CRN ages from boulders on associated moraine ridges. The environment of deposition of the sediment collected was determined by comparing the geomorphology and lithofacies associations with the land systems models and lithofacies associations developed in Owen (1993, 1996).

2.1. Location A

Sample UCR_055 was collected from an exposure in a succession of sands and silts within a series of moraine ridges of the Ghulkin II Glacial Stage (t5) ~2 km east of the Pasu glacier (Figs. 2A and 3A). These sediments were deposited in a shallow glaciolacustrine pond that probably formed shortly after the Ghulkin II glaciation.

2.2. Location B

A high cliff above the Hunza River, ~2 km east of the Pasu glacier, exposes a succession of fluvial, glaciofluvial and lacustrine sediments that are overridden by deformation till of Ghulkin I Glacial Stage (t4). Sample

UCR_056 was collected from deformed medium to fine-grained sands and silts immediately below the deformation till (Figs. 2B and 3B).

2.3. Location C

A succession of glaciolacustrine sediments overlain by till of the Batura Glacial Stage (t6) is exposed along the valley wall ~1 km west of Pasu village (Figs. 2C and 3C). Sample UCR_057 was collected from cm-thick beds of medium to fine-grained sands that are interbedded with crudely laminated cm- to dm-thick planar beds of massive silts.

2.4. Location D

A small gravel pit ~2.5 km southeast of the Batura glacier exposes a succession of glaciolacustrine and glaciofluvial sands and silts that are overlain by till of the Ghulkin II Glacial Stage (t5) (Figs. 2D and 3D). Sample UCR_059 was collected from finely laminated cm-thick planar beds of sands and silts.

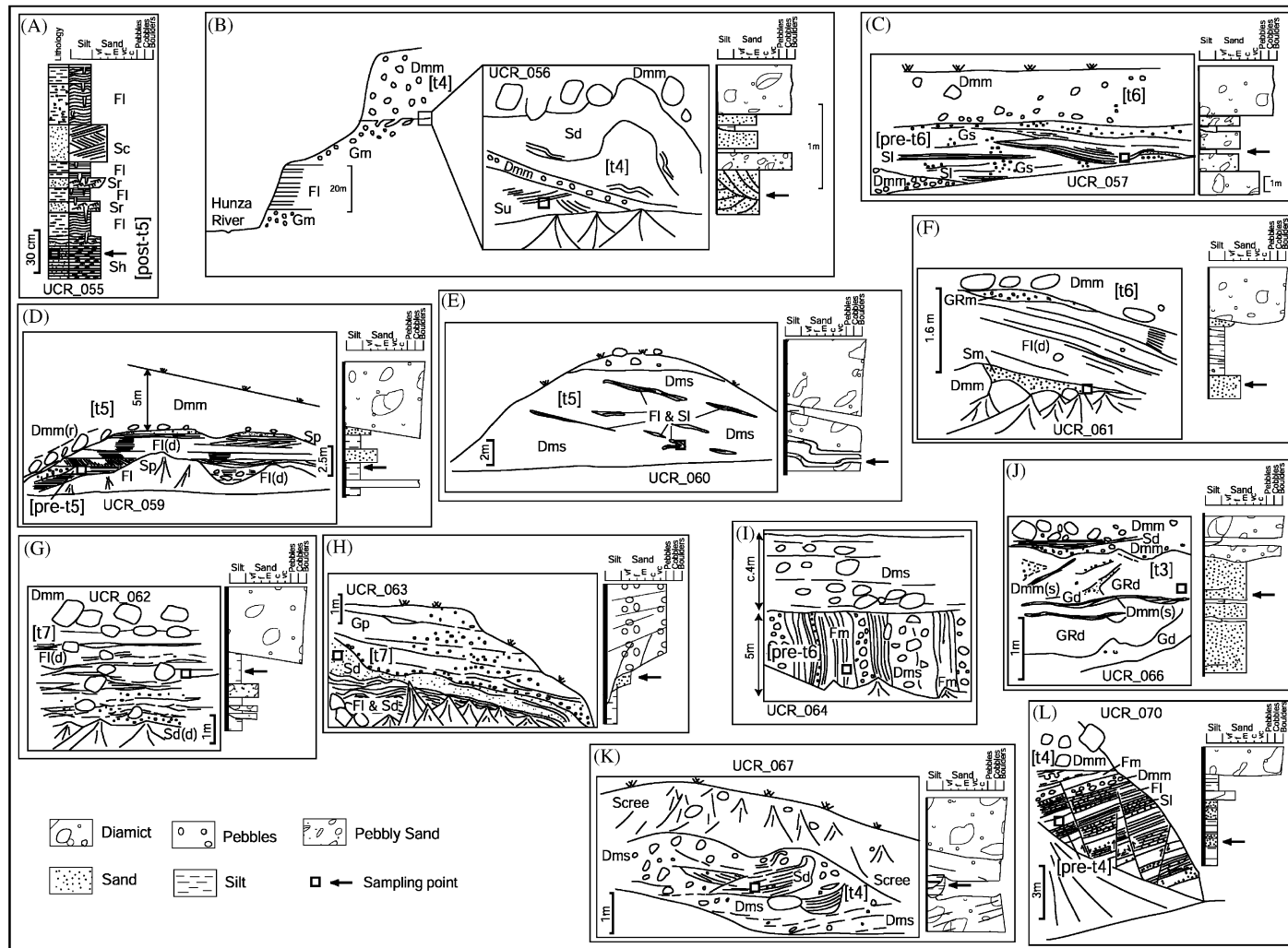


Fig. 2. Lateral and vertical graphic sedimentary logs showing the positions of where sediment samples were collected for OSL dating. (A) Glaciolacustrine sediments overlying t5 moraines ($36^{\circ}27.478'N/74^{\circ}54.435'E$, 2480 m asl). (B) Deformed glaciofluvial sediments beneath t4 tills ($36^{\circ}27.109'N/70^{\circ}54.126'E$, 2540 m asl). (C) Glaciolacustrine sediments underlying t6 till ($36^{\circ}28.159'N/74^{\circ}53.496'E$, 2550 m asl). (D) Glaciolacustrine sediments underlying t5 till ($36^{\circ}29.942'N/74^{\circ}52.993'E$, 2550 m asl). (E) Latero-frontal moraine of t5 ($36^{\circ}29.920'N/74^{\circ}53.103'E$, 2560 m asl). (F) Glaciolacustrine sediments beneath t6 tills ($36^{\circ}30.169'N/74^{\circ}53.097'E$, 2610 m asl). (G) Deformation till of t7 ($36^{\circ}30.269'N/74^{\circ}51.836'E$, 2575 m asl). (H) Glaciofluvial sediments within a t7 latero-frontal moraine ($36^{\circ}30.341'N/74^{\circ}52.003'E$, 2565 m asl). (I) Pre-t6 age glaciotectionized glaciofluvial sediments underlying debris flow sediments ($36^{\circ}30.490'N/74^{\circ}52.881'E$, 2530 m asl). (J) t3 deformation till ($36^{\circ}26.110'N/74^{\circ}51.531'E$, 2650 m asl). (K) t4 lateral moraine ($36^{\circ}26.537'N/74^{\circ}52.202'E$, 2560 m asl). (L) Glaciotectionized glaciofluvial sediments underlying t4 till ($36^{\circ}24.312'N/74^{\circ}52.468'E$, 2340 m asl). Lithofacies codes following Eyles et al. (1983) are used to describe the sedimentology (Dmm—massive matrix-supported diamict; Dmm(r)—resedimented, massive matrix-supported diamict; Dmm(s)—sheared, massive matrix-supported diamict; Dms—stratified, matrix-supported diamict; FI—laminated silt; FI(d)—fine-grained laminated sands or silts with dropstones; Fm—massive, fine-grained sands or silts; Gd—deformed pebbly sand; Gm—massive or crudely bedded gravel; Gp—stratified gravel with planar crossbedding; GRd—deformed massive beds of pebbly sand; GRm—massive and homogeneous granules; Gs—stratified gravels; Sc—fine to coarse sands with planar cross-stratification; Sd—deformed sands; Sd(d)—deformed sands with dropstones; Sh—horizontally laminated, very-fine to coarse sands; SI—laminated sands; Sm—massive sands; Sp—medium to very-coarse sands; Sr—rippled, very-fine to coarse sands; Su—trough cross-stratified sands).

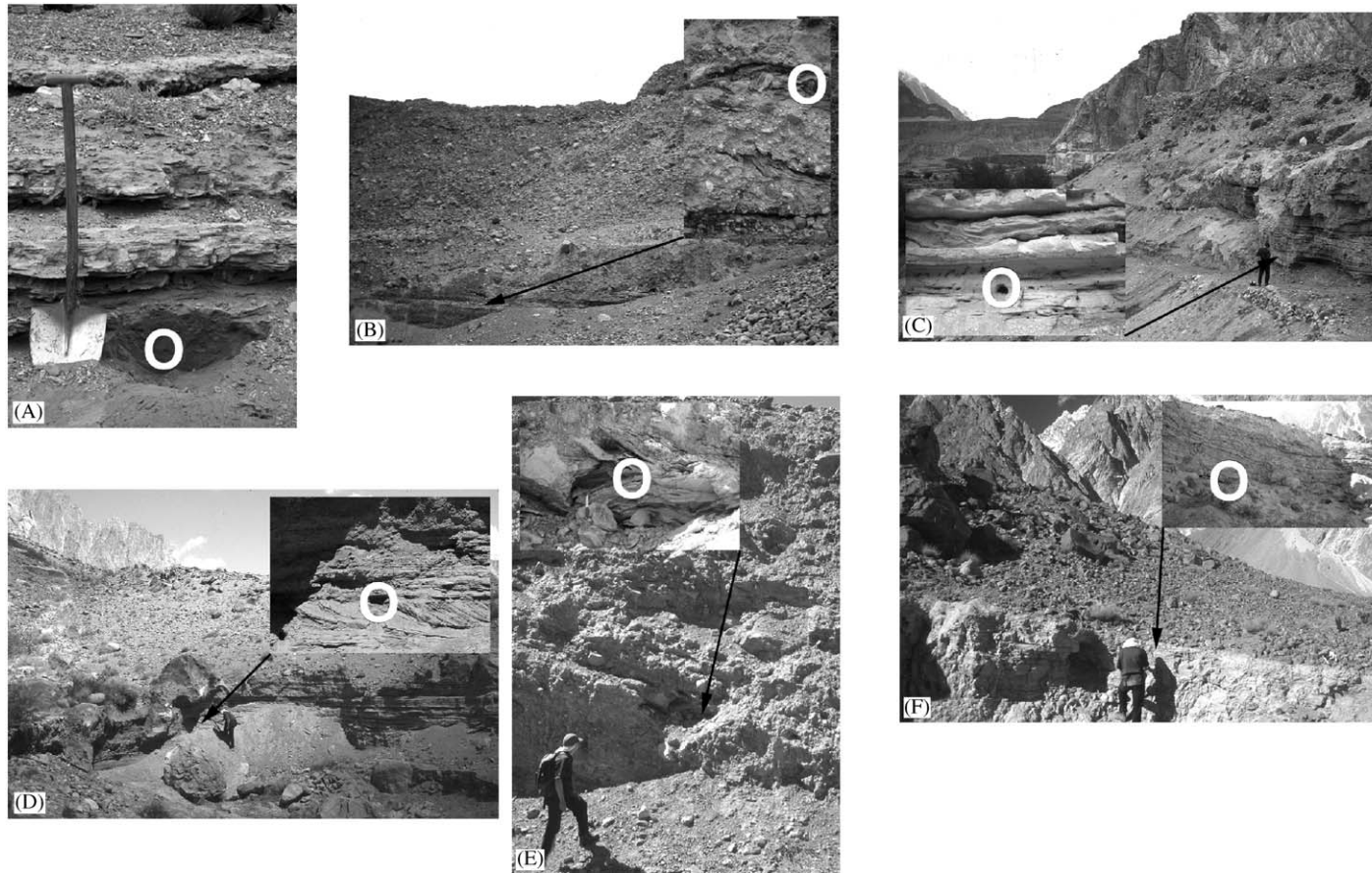


Fig. 3. Plates showing the locations and sampling positions (white circles) for OSL dating samples UCR_055, 056, 057, 059, 060, 061, 062, 063, 064, 066, 067 and 070. (A) View looking northwards at an exposure in glaciolacustrine sediments within a depression in moraines of t5 age ($36^{\circ}27.478'N/74^{\circ}54.435'E$, 2480 m asl; UCR_055). (B) View looking west at deformed glaciofluvial sediments beneath t4 tills in a high cliff above the Hunza River ($36^{\circ}27.109'N/70^{\circ}54.126'E$, 2540 m asl; UCR_056). (C) View looking NW at glaciolacustrine sediments underlying t6 till ($36^{\circ}28.159'N/74^{\circ}53.496'E$, 2550 m asl; UCR_057). (D) View looking east at glaciolacustrine sediments underlying t5 till in a small gravel pit ($36^{\circ}29.942'N/74^{\circ}52.993'E$, 2550 m asl; UCR_059). (E) View looking north at a section through a latero-frontal moraine of t5 age ($36^{\circ}29.920'N/74^{\circ}53.103'E$, 2560 m asl; UCR_060). (F) Exposure within glaciolacustrine sediments beneath t6 tills ($36^{\circ}30.169'N/74^{\circ}53.097'E$, 2610 m asl; UCR_061). (G) View NNE at deformation till of t7 ($36^{\circ}30.269'N/74^{\circ}51.836'E$ 2575 m asl; UCR_062). (H) View looking WSW at glaciofluvial sediments of t7 age within a latero-frontal moraine ($36^{\circ}30.341'N/74^{\circ}52.003'E$, 2565 m asl; UCR_063). (I) View looking ESE at pre-t6 age glaciotectionized glaciofluvial sediments underlying debris flow sediments ($36^{\circ}30.490'N/74^{\circ}52.881'E$, 2530 m asl; UCR_064). (J) View looking north at an exposure in deformation till of t3 age ($36^{\circ}26.110'N/74^{\circ}51.531'E$, 2650 m asl; UCR_066). (K) View looking north at an exposure in an irrigation dyke that traverses a lateral moraine of t4 age ($36^{\circ}26.537'N/74^{\circ}52.202'E$, 2560 m asl; UCR_067). (L) View looking north at a road cutting through glaciotectionized glaciofluvial sediments underlying t4 till ($36^{\circ}24.312'N/74^{\circ}52.468'E$, 2340 m asl; UCR_070).

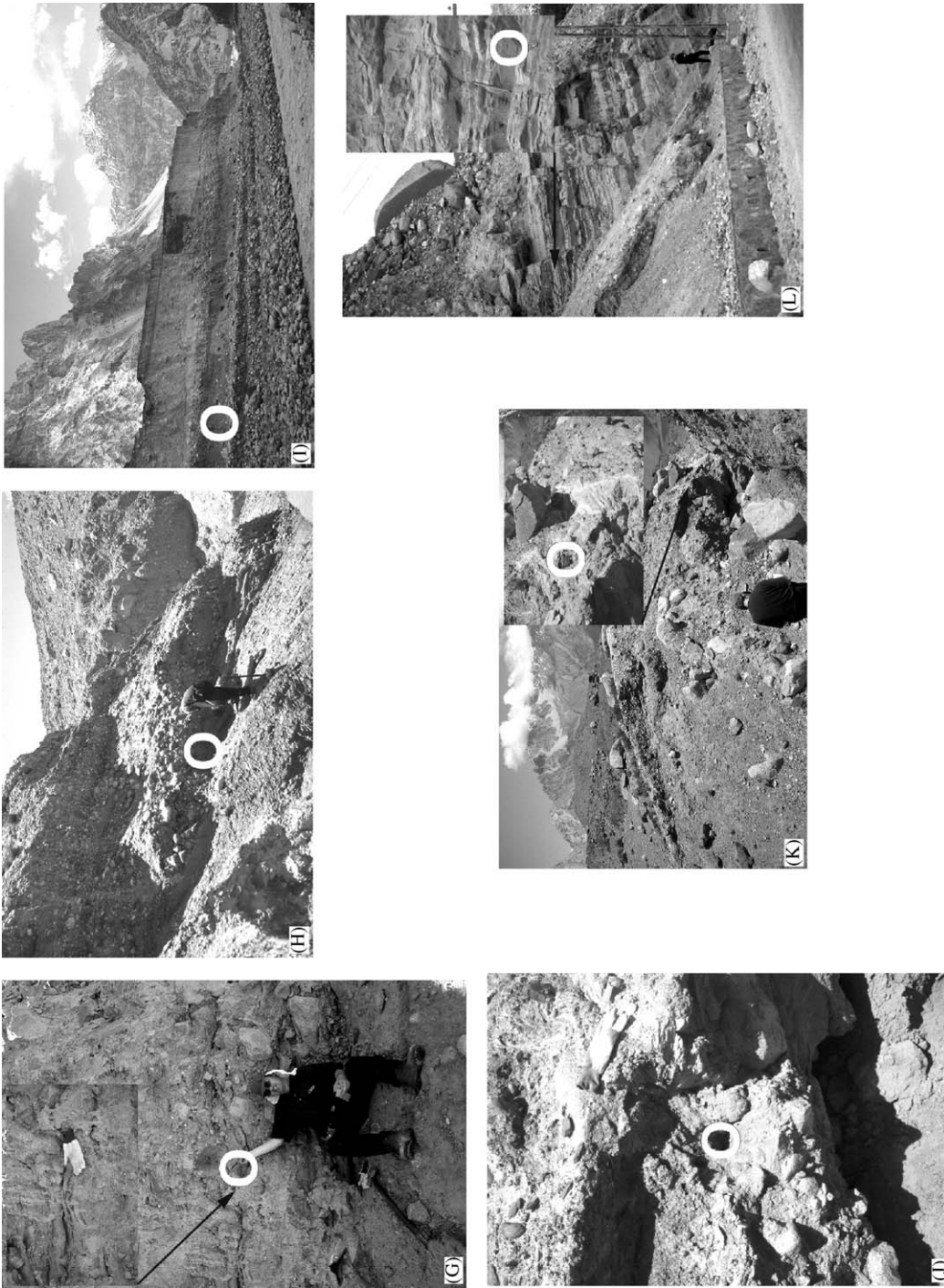


Fig. 3 (continued).

2.5. Location E

A road cutting through the ridge of a latero-frontal moraine complex of the Ghulkin II Glacial Stage (t5) ~3 km southeast of the Batura glacier exposes diamicts and deformed lenses of supraglacial lacustrine sands and silts (Figs. 2E and 3E). Sample UCR_060 was collected from within a lens of folded laminated sands and silts.

2.6. Location F

An exposure ~2.5 km east of the Batura glacier exposes slumped glaciolacustrine silts and sands that are overlain by slumped supraglacial meltout till of the Batura Glacial Stage (t6) (Figs. 2F and 3F). Sample UCR_061 was collected from a fine to medium grained massive sand bed at the base of the section.

2.7. Location G

An exposure ~200 m from the snout of the Batura glacier exposes deformation tills of the Pasu I Glacial Stage (t7) that overlie deformed glaciolacustrine sediments (Figs. 2G and 3G). Sample UCR_062 was collected from a deformed sand lens that was interbedded within deformed silts.

2.8. Location H

An exposure near the snout of the Batura glacier exposes a succession of slumped proglacial glaciolacustrine sandy silts and glaciofluvial sands and gravels (Figs. 2H and 3H). Sample UCR_063 was collected from a stratified bed of medium sands.

2.9. Location I

The truncated toes of an alluvial fan along the northern side of the Hunza River southeast of the Batura glacier, exposes glaciotectionized glaciofluvial sediments that lie almost vertically due to deformation during the Batura Glacial Stage (t6) and are unconformably overlain by debris flow deposits (Figs. 2I and 3I). Sample UCR_064 was collected from massive planar beds of silt.

2.10. Location J

An exposure in a degraded moraine ~200 m west of Borit Jheel reveals a succession of stratified matrix-supported diamict with deformed massive beds of pebbly sand (Figs. 2J and 3J). Sample UCR_066 was collected from a massive sand bed that contains occasional pebbles.

2.11. Location K

An irrigation canal through a moraine ridge of the Borit Jheel Glacial Stage (t3) exposes a succession of supraglacial till and deformed glaciofluvial sands and gravels (Figs. 2K and 3K). Sample UCR_067 was collected from within a deformed lens of cm-thick beds of cm- and mm-size planar beds of pebbly silts.

2.12. Location L

A road cutting ~1 km south of the Ghulkin glacier reveals supraglacial till of the Ghulkin I Glacial Stage (t4) overlying faulted fluvial sands and gravels (Figs. 2L and 3L). Sample UCR_070 was collected from a dm-thick planar bed of silty sand.

3. Sampling and sample preparation

The OSL samples were obtained by hammering opaque plastic tubes into cleaned sections; two block samples were excavated from sections that were too compact to enable insertion of sampling tubes. Once removed the samples were sealed in plastic and placed in light-tight sampling bags. Smaller sub-samples were collected from the same locations to enable replication of water content measurements and for environmental dose-rate assessment (see Section 4 below). All the samples remained sealed until opened in the laboratory.

At the luminescence laboratories at the University of California, Riverside, the sediment from the 10 tube-samples was carefully removed. About 2–3 cm of sediment, which may have been exposed to daylight during sampling, was removed from the ends of the tube before the sediment used for dating was extracted. To ensure sediment was not wasted, and avoid daylight-exposed material, the block samples were sprayed with black paint, left to dry, and then the painted surfaces were carefully removed (Rhodes, pers. comm.). Estimates of in situ water content (mass of moisture/dry mass; Aitken, 1998) were calculated by recording the mass of sediment before and after dry weight stabilization in a 50°C oven; these measurements were also made on the sub-samples. The samples for dating were dry sieved to obtain a 90–125 µm particle size fraction. In certain cases a hard concretion formed during drying, and after an initial procedure of gentle crushing, sieving and removal and retention of the <90 µm fraction, wet sieving was employed to remove finer material and increase coarser sieve fraction yields. After wet sieving, the individual sieves were dried in a 50°C oven and the sediment was dry-sieved once again.

The carbonates and organic matter were removed from the 90–125 µm fraction utilizing 10% HCl and 30% H₂O₂, respectively. The 90–125 µm fractions were then washed several times in distilled H₂O and then

treated with 10% HF for 30 min. This acid wash removed the outer few microns from the surface of the feldspathic grains, thereby minimizing the infrared stimulated luminescence (IRSL) signal from feldspar due to ionization by alpha particles; additionally, by washing the whole sample in 10% HF at this stage, we obtained significantly improved mineral separation. A 10% HCl wash was administered to dissolve any precipitated fluorides, and the samples were then washed in H₂O and acetone and briefly dried in a 50°C oven. Sodium polytungstate solutions of appropriate densities and a centrifuge were used to separate the quartz and feldspar-rich fractions from the heavy minerals. The density fractions were washed in H₂O and acetone and dried. The separated quartz-rich fraction (2.62–2.74 g cm⁻³) was treated with 49% HF for 30 min to dissolve plagioclase feldspars; similar to the HF etch of feldspar minerals, this acid wash minimized the luminescence from alpha particles. Some of the quartz samples were given an additional 30 min wash in HF or a 7-day treatment in 35% H₂SiF₆ to reduce the IRSL signal (see below) from contaminant feldspar to a negligible level. After HF or H₂SiF₆ treatment the quartz-rich fractions were given a 10% HCl wash to dissolve any precipitated fluorides, and final H₂O, acetone and drying steps. K-feldspar (2.51–2.58 g cm⁻³) and quartz grains were dispensed onto stainless steel discs (10 mm in diameter) coated with a layer of silicone spray. All preparation techniques were carried out under laboratory safelights (cf. Spooner et al., 2000) to avoid bleaching of the natural (Quaternary) luminescence.

4. Determination of environmental dose-rate

About 20 g from each dried sub-sample was ground to a fine powder using a pestle and mortar and sent to the

Bequerel Laboratories in Australia for Neutron Activation Analysis (NAA) to determine the concentrations of U, Th, K and Rb (Table 2). Using appropriate dose-rate conversion factors (Adamiec and Aitken, 1998) and beta attenuation factors (Mejdahl, 1979; see Table 3, footnote c) the elemental concentrations were converted into external beta and gamma components, which were in turn attenuated for moisture content. These were summed together with a cosmic ray component (estimated using Prescott and Hutton, 1994; Table 2) to give estimates of the total dose-rate from each sample (Table 3).

Although an assessment of secular disequilibrium was not carried out, for all of the samples the U concentration (Table 2) contributes a smaller fraction of the total dose-rate compared to typical silt/sand sediments (e.g. 3 ppm U, 10 ppm Th, 1.5% K), and, therefore, even if acute (e.g. 50%) disequilibrium in the U series is present we would expect any additional uncertainty in dose-rate to be significantly less than 8% (Olley et al., 1996). Whenever possible homogeneous single-texture sediment exposures extending to a radius of > 30 cm around the sampling position were selected. This was carried out to minimize uncertainty in the gamma dose-rate from NAA data. For samples UCR_066 and UCR_067 (locations J, Figs. 2J and 3J and location K, Figs. 2K and 3K, respectively) the sediment contained pebble-sized clasts, and therefore representative portions of these clasts were included in the 20 g sample for NAA. For UCR_063, the location in the sandy horizon from which the sample was removed was, approximately, between 5 and 15 cm from a glaciofluvial deposit (Figs. 2H and 3H), and therefore there is a possible additional uncertainty associated with the estimation of the gamma dose-rate. Similarly, UCR_062 was collected < 30 cm from dropstones ~15–20 cm in size (Figs. 2G and 3G), although in this case both the sands from the sampling

Table 2
Sample locations, radioisotope concentrations, moisture contents and calculated cosmic ray dose-rates

UCR lab no.	Location (N, E)	asl (m)	Depth (m)	U ^a (ppm)	Th ^a (ppm)	K ^a (%)	Rb ^a (ppm)	W _{in situ} ^b (%)	Cosmic ^c (m Gya ⁻¹)
062	36°30.27', 74°51.84'	2575	17	2.32	17.2	2.30	97.8	0.12	0.061
063	36°30.34', 74°52.00'	2565	1	2.19	13.5	1.85	94.9	0.27	0.278
061	36°30.17', 74°53.10'	2610	1.5	3.37	12.8	1.64	85.5	0.99	0.264
064	36°30.49', 74°52.88'	2530	40	5.46	15.1	2.97	202.0	0.43	0.027
057	36°28.16', 74°53.50'	2550	5	2.25	13.3	1.66	97.4	0.56	0.178
055	36°27.48', 74°54.44'	2480	0.30	2.71	13.6	1.83	95.3	0.95	0.301
060	36°29.92', 74°53.10'	2560	8	2.68	11.6	1.40	69.3	0.39	0.130
059	36°29.94', 74°52.99'	2550	1.5	2.14	11.0	1.17	54.3	2.50	0.261
056	36°27.11', 74°54.13'	2540	10	2.76	12.5	1.59	84.2	0.36	0.108
067	36°26.54', 74°52.20'	2560	2.4	2.11	16.1	1.20	63.3	0.69	0.238
070	36°24.31', 74°52.47'	2340	10	2.22	13.9	1.71	88.7	0.25	0.104
066	36°26.11', 74°51.53'	2650	3	2.87	17.9	1.88	83.0	0.56	0.226

^aElemental concentrations from NAA of whole sediment measured at Becquerel Laboratories, Lucas Heights, NSW, Australia. Uncertainty taken as ±10%.

^bEstimated fractional water content from whole sediment (Aitken, 1998). Uncertainty taken as ±5%.

^cEstimated contribution to dose-rate from cosmic rays calculated according to Prescott and Hutton (1994). Uncertainty taken as ±10%.

location and the dropstones were assessed to have the same granitic lithology. Regarding possible heterogeneity in beta dose-rate, the 20 g sub-samples were collected from exactly the same locations as the OSL samples and size distribution indicates silt and clay-sized particles are not dominant in the majority of samples. We therefore consider additional uncertainty due to differences in beta dose-rate from clays, silts and sands to be minimized. A further factor to consider is time-dependent beta dose-rate variation due to the mobility of K; K has shown to be enhanced in the runoff from glacial environments compared to non-glacial environments (e.g., Anderson et al., 1997). However, the enhancement in K is more likely to occur due to weathering of bedrock surfaces after glacial abrasion, rather than weathering of minerals in the moraine subsequent to emplacement.

5. OSL measurements

Luminescence measurements were undertaken using a Daybreak 1100 automated system with an 1100FO/L combined fiber-optic/IRLED illuminator for optical stimulation (Bortolot, 1997). Luminescence from the K-feldspar grains was measured using infrared stimulation from T-1 GaAlAs diodes (880Δ80 nm; diode current 20 mA). Luminescence from the quartz grains was stimulated using a 150 W halogen lamp producing either a broadband blue-green light ($\sim 425\text{--}600\text{ nm}$; $\sim 72\text{ mW cm}^{-2}$) using the basic excitation filter stack or a green light (514Δ34 nm; $\sim 20\text{ mW cm}^{-2}$) defined by an additional narrow band interference filter. All quartz samples were screened for feldspar contamination using the infrared diode array. The blue-green stimulated luminescence (BGSL) or green-light stimulated luminescence (GSL) signals from quartz were detected with a photomultiplier tube using 9 mm Schott UG11 ultraviolet detection filters. For the IRSL signals from K-feldspar the detection filters used were a combination of Schott BG39 and Corning 7-59; these filters transmit principally in the blue-violet part of the visible spectrum. The IRSL data were analyzed using a combination of Microsoft Excel and Jandel Scientific SigmaPlot. The GSL and BGSL data were analyzed using Daybreak TLApplic 4.26 software and Microsoft Excel.

Single-aliquot protocols were used to determine equivalent dose (D_e) estimates for K-feldspar and quartz minerals. In this approach repeated cycles of laboratory irradiation, preheating and luminescence measurement were made on a single disc (aliquot) of the same sample. The preheating steps were incorporated to remove unstable components in the luminescence signal. For the K-feldspar minerals a single-aliquot additive dose (SAAD) procedure was used (Duller, 1991, 1994), where the measured data were corrected for the loss of signal

due to the repeated preheat and optical stimulation cycles on the same aliquot. A preheat of 220°C for 10 min (cf. Li, 1991) was used. Infrared stimulation comprised short-shines of 440 ms, ensuring that only a small proportion of the total signal was removed during each measurement cycle. The correction procedure was carried out by comparing the IRSL short-shine data from the additive dose cycles with the depletion in IRSL observed during a preheat calibration; the preheat calibration comprised only preheat and IRSL short-shine cycles on a duplicate aliquot. Background luminescence levels, assessed by IRSL measurement on each sample after thermal removal (to 450°C) of the optical signal, were subtracted from the additive dose and preheat calibration data before correction. Either a linear or saturating exponential function was fitted to the corrected additive dose data, and D_e values estimated by extrapolating the curve to zero luminescence intensity.

For the quartz minerals, D_e estimates were determined using the single-aliquot regenerative-dose (SAR) protocol developed by Murray and Wintle (2000). In the SAR method, each natural or regenerated GSL or BGSL signal is corrected for changes in sensitivity using the luminescence response to a subsequent test dose. The natural dose (N) was measured in the first cycle, and thereafter five regeneration doses ($R_1\text{--}R_5$) were administered. The first three were used to bracket the natural luminescence level ($R_1 < N \sim R_2 < R_3$), the fourth (R_4) was set at zero to monitor thermal transfer (i.e. R_4/N) and the fifth dose was made equal to the first to monitor reproducibility of sensitivity corrections (i.e. R_5/R_1). Each measurement cycle comprised a regeneration dose (zero for natural), a preheat of 200°C for 10 s, optical stimulation for 100 s (sample temperature of 125°C), a constant test-dose, a test-dose cut-heat of 160°C and a final optical stimulation for 100 s (at 125°C). The net-natural and net-regenerated OSL were derived by taking the initial OSL signal (0–1 s) and subtracting a background from the last part of the stimulation curve (90–100 s); the net test-dose response was derived by subtracting, from the initial OSL signal, the background from the preceding natural and regenerative OSL signals. Multiple D_e estimates were carried out on each sample. Growth curves were plotted using the net-regenerated data divided by the subsequent response to the net-test dose. The growth curve data were fitted with a single saturating exponential function and D_e estimates evaluated by interpolation with the natural sensitivity-corrected luminescence level. Two rejection criteria were utilized; if thermal transfer was $> 5\%$ of the natural level and if the mean recycling ratio between repeat regenerative doses was < 0.9 or > 1.1 (Murray, pers. comm.) with allowance for uncertainty in recycling. The distribution in D_e values was assessed using histogram plots (e.g. Fig. 6).

Tests of neighbouring disc cross-illumination in the Daybreak system were carried out using adjacent discs of calibration quartz by measuring a full SAR protocol on the first measured disc, first neighbouring disc, second neighbouring disc, and third neighbouring disc, in turn, and calculating the depletion in D_e compared to the first measured disc. Measurement was by GSL (514 nm) with a cumulative shine time for each disc of 1200 s. Depletion in D_e was highly significant at $\sim 13\%$ for the first neighbouring disc, $\sim 19\%$ for the second neighbouring disc, and $\sim 23\%$ for the third neighbouring disc. Further tests demonstrated that the number of discs on the 20-position turntable was limited to only a single disc for BGSL and to 4 discs (with 90° separation) for GSL. Due to the pressure this introduced on machine and user time, preheat plateaux were not investigated. Although we cannot exclude the possibility that there is some preheat dependence on our D_e results, observations by Rhodes (2000) of thermal transfer phenomena in glaciogenic sediments tend to justify use of a relatively low preheat temperature, and therefore the 200°C preheat described above was used in this work. Due to firmware constraints < 1 s optical stimulation integrals were not investigated.

6. Results

6.1. K-feldspar IRSL

Examples from two of the SAAD luminescence growth curves are shown in Fig. 4. Both indicate a non-linear response to added beta dose, as do a further seven of the 12 K-feldspar samples measured. For the majority of these samples it was either not feasible or impracticable in machine time to achieve a desired cumulative additive-dose luminescence level of ~ 4 – 5 times the natural level to reduce extrapolation uncertainty. Apart from UCR_055 (Fig. 4a) and UCR_060, the highest cumulative dose-corrected (Duller, 1994) point is for sample UCR_059 at only ~ 3 times the natural level. The remaining non-linear growth curves have values between ~ 1.6 – 2.5 times the natural level (UCR_056, UCR_057, UCR_064, UCR_067 and UCR_070), and the lowest value is ~ 0.76 for sample UCR_066, even after an actual cumulative added-dose of more than 3500 Gy; subsequent to dose-correction (Duller, 1994), the effective added beta dose is ~ 3000 Gy (Fig. 4b). Furthermore, the non-linear curves show that the luminescence signal is saturating even though the growth in signal is relatively poor; this is particularly apparent for sample UCR_066 (Fig. 4b) and also samples UCR_064, UCR_067 and UCR_070.

6.2. Quartz GSL and BGSL

Examples of the SAR growth curves from samples UCR_055 and UCR_066 are shown in Fig. 5. In these

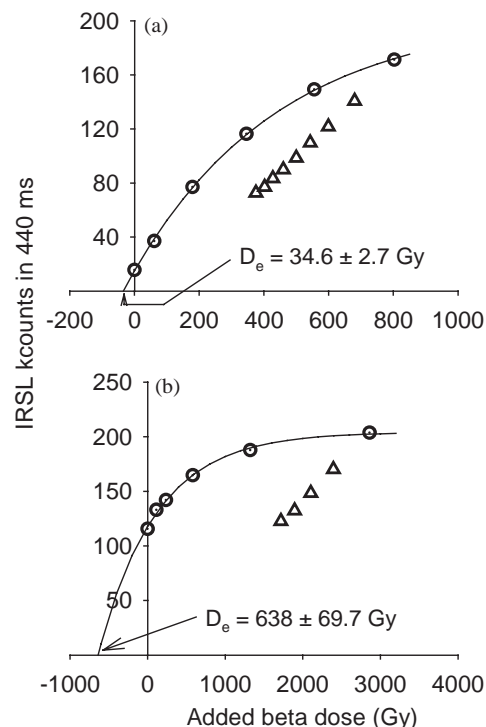


Fig. 4. Examples of SAAD growth curves from 90–125 μm K-feldspar. The dose correction method (Duller, 1994) and extrapolation using a single saturating exponential function was used to estimate the D_e value. (a) UCR_055; (b) UCR_066. The disconnected sets of points (open diamonds) are the replicated highest additive dose measurements.

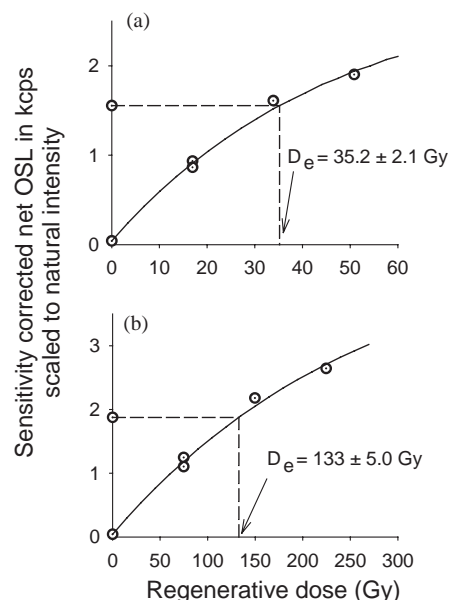


Fig. 5. Examples of SAR (Murray and Wintle, 2000) growth curves from 90–125 μm quartz. A single saturating exponential function was used to fit the curves (solid lines) through the regenerative dose points. The D_e values were estimated by interpolation (dashed lines). (a) UCR_055; (b) UCR_066.

Table 3

Summary of OSL dating results from 90–125 μm quartz extracted from sediment matrices: comparison with CRN results from Owen et al. (2002a)

UCR lab no.	Quartz OSL results				Relation between OSL age and till unit (cf. Fig. 2)	CRN age range from Owen et al. (2002a) (ka)
	n^a	Mean D_e^b (Gy)	Dose-rate ^c (m Gya ⁻¹)	Age ^d (ka)		
062	5(16)	17.8 ± 1.2	4.12 ± 0.27	4.3 ± 0.4 [?]	t7	No data
063	10(13)	30.1 ± 2.7	3.57 ± 0.22	8.4 ± 0.9	t7	No data
061	5(7)	27.9 ± 1.8	3.58 ± 0.21	7.8 ± 0.7	Maximum t6	9.0–10.8
064	1(15)	122 ± 17	5.36 ± 0.35	22.8 ± 3.6 [?]	Pre-dates t6	9.0–10.8
057	6(6)	93.2 ± 6.8	3.27 ± 0.20	28.5 ± 2.7	Pre-dates t6	9.0–10.8
055	8(8)	32.2 ± 2.2	3.70 ± 0.22	8.7 ± 0.8	Post-dates t5	15.3–18.4
060	12(12)	35.8 ± 2.5	2.98 ± 0.18	12.0 ± 1.1	t5	15.3–18.4
059	9(13)	47.7 ± 3.5	2.65 ± 0.15	18.0 ± 1.7	Pre-dates t5	15.3–18.4
056	6(10)	59.0 ± 3.7	3.20 ± 0.20	18.4 ± 1.6	Maximum t4	21.8–25.7
067	5(17)	96.3 ± 7.2	3.05 ± 0.18	31.5 ± 3.0	t4	21.8–25.7
070	4(13)	146 ± 14	3.29 ± 0.21	44.4 ± 5.2 [?]	Pre-dates t4	21.8–25.7
066	3(16)	126 ± 11	3.99 ± 0.24	31.6 ± 3.3 [?]	t3/t4?	21.8–25.7/43.2–54.7

^a Number of replicated D_e estimates used to calculate mean D_e . Figures in parentheses indicate total number of D_e measurements made including failed runs with unusable data.

^b Mean D_e determined from replicated single-aliquot regenerative-dose (SAR; Murray and Wintle, 2000) runs. Errors are 1-sigma standard errors (i.e. $\sigma_{n-1}/n^{1/2}$) incorporating ± 5% uncertainty in beta source calibration.

^c Total dose-rate from beta, gamma and cosmic ray components. External beta attenuation factors for U, Th and K compositions calculated using Rainer Grün’s “Age” program incorporating grain size factors from Mejdahl (1979). Beta attenuation factor for Rb arbitrarily taken as 0.75 (cf. Adamiec and Aitken, 1998). Factors utilized to convert elemental concentrations to beta and gamma dose-rates from Adamiec and Aitken (1998) and beta and gamma components attenuated for moisture content.

^d Results marked with a question mark (?) are considered possibly erroneous due to high thermal transfer (UCR_062) and low number of repeat D_e s principally due to failure of SAR sensitivity correction (UCR_064, UCR_066, UCR_070).

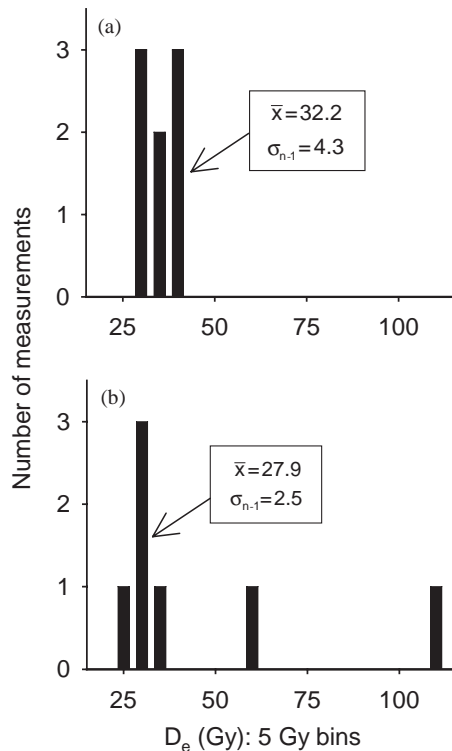


Fig. 6. Histograms of distributions in D_e values from quartz-SAR measurements. (a) UCR_055 and (b) UCR_061.

examples, the recycling ratio lies within 0.9–1.1 indicating that the SAR protocol had adequately corrected for changes in luminescence sensitivity. However, in 5 out of

the 12 samples, several individual SAR measurements, which increased the mean recycling ratio above 1.1 or below 0.9, were rejected. For UCR_062, 6 out of 16 measurements were rejected with recycling ratios varying from 0.28 to 0.78 and 1.18 to 4.90; UCR_067, 7 out of 17 with values from 0.61 to 0.76; UCR_070, 8 out of 13 with values from 0.60 to 0.78; UCR_066, 12 out of 16 with values from 0.57 to 0.77; and UCR_064, 13 out of 15 with values from 0.29 to 0.74. Some of the above figures, for example the high value of 4.90 for one of the UCR_062 aliquots, were due to low signal intensities from GSL. Luminescence levels from certain samples were somewhat improved for further aliquots by removing the 514 nm interference filter which increased stimulation power and broadened the waveband to blue-green (~425–600 nm) stimulation.

For the majority of samples, thermal transfer was only a few percent of the natural luminescence level and very rarely reached the 5% rejection level (e.g. Fig. 5). However, for sample UCR_062 thermal transfer was a more significant factor. If we ignore probable anomalous thermal transfer due to low signal levels by, for example, setting the minimum allowable signal-to-noise ratio at ~3 (allowing a maximum ± 10% uncertainty in net photon counts), we still retain a range of thermal transfer values from 8.7% to 13.1% of the natural dose for UCR_062.

Examples of histograms of the distribution in D_e values are shown in Fig. 6. Fig. 6a shows the result for sample UCR_055. The eight D_e measurements cluster

reasonably tightly and therefore all the values were used to calculate a mean of 32.2 Gy with a standard deviation of 4.3 Gy. In contrast, in Fig. 6b (UCR_061) there is clearly a broad distribution of D_e values, although the majority of the data clusters towards lower D_e values of 25–35 Gy and there are only two points with much higher D_e values. In this case, the lowest dose population was used to calculate a mean D_e of 27.9 Gy with a standard deviation of 2.5 Gy. The basis for taking the average of this low-dose population is due to the effects of partial bleaching, and the justification for this approach is provided later. Similar D_e distributions with clustered points at a minimum D_e value were present in histograms in all the samples studied. The mean D_e values for these refined data sets are shown in Table 3.

6.3. Comparison of K-feldspar IRSL and quartz GSL and BGSL

Comparison of the results between K-feldspar and quartz measurements for UCR_055 (Fig. 4a and 5a, respectively) shows excellent concordance in D_e values: 34.6 ± 2.7 (K-feldspar) and 35.2 ± 2.1 Gy (quartz). These measurements correspond to ages of 8.3 ± 1.0 ka for the feldspar and 8.7 ± 0.8 ka for the quartz, using the mean quartz D_e for UCR_055 of 32.2 ± 2.21 Gy from Table 3. Similarly, the K-feldspar and quartz results for UCR_060 are highly concordant with D_e values of 38.8 ± 5.0 and 35.8 ± 2.5 Gy, and ages of 11.3 ± 1.8 and 12.0 ± 1.1 ka, respectively. The concordance between quartz and K-feldspar results for UCR_055 and UCR_060 may indicate that anomalous fading is either not present or has a minor effect on the feldspars from these two samples, although further feldspar measurements are required to confirm this observation. In contrast to UCR_055 and UCR_060, clearly there is considerable discordance between the K-feldspar (Fig. 4b) and the quartz (Fig. 5b) results for UCR_066. The same disparity between mineral ages is shown in every other sample, where the feldspar age is significantly higher than the corresponding quartz age. Furthermore, the shape of the K-feldspar growth curve for sample UCR_066 (Fig. 4b), and possibly samples UCR_064 and UCR_070, may indicate dynamic equilibrium conditions (cf. Mejdahl, 1988), which suggests D_e underestimation and thus even greater disparity between quartz and feldspar ages for these samples.

7. Discussion

7.1. Assessment of OSL methods

The non-linear K-feldspar-SAAD growth curves indicate that only samples with good agreement with

quartz SAR D_e values (UCR_055; Figs. 4a and 5a; and UCR_060) have highest cumulative dose points >4–5 times the natural luminescence level. The remaining samples all have values <3 times the natural level and the onset of saturation is evident even though the luminescence growth is poor. This is an indication of the presence of large remnant geological luminescence signals, suggesting inadequate bleaching of the infrared signal before deposition and overestimation of the feldspar ages. Because the K-feldspar-SAAD growth curves for samples UCR_061, UCR_062 and UCR_063 are linear, we have no evidence to suggest partial bleaching. However, the K-feldspar ages for these samples are higher by a factor of between ~1.6 and 3.5 in comparison with ages from quartz-SAR, and the quartz data are derived from mean D_e values from clustered low dose populations (Table 3). Since the K-feldspar work described here was from a preliminary assessment, eight of the results are only from two repeats, and the remaining four only from a single measurement, we therefore are not able to examine the extent of D_e distribution. However, based on the evidence of signal saturation (e.g. Fig. 4b) and due to the wide discordance demonstrated for 10 out of the 12 samples (e.g. Figs. 4b and 5b) compared with the mean D_e calculated from multiple quartz SAR results (Table 3), we assess that in most cases K-feldspars are unsuitable for dating glaciogenic sediments, or glaciogenic sediments from this region, due to inadequate bleaching. Furthermore, recent optical dating studies that we have conducted on Late Quaternary glaciation in the Chitral valley in the eastern Hindu Kush range of northern Pakistan (Owen et al., 2002b) draw the same conclusion. Although Preusser (1999) observed similar rapid bleaching rates for quartz and feldspar, other studies suggest possible mineral dependence in bleachability (e.g. summarized by Aitken, 1998, p. 151), as we believe the preliminary findings in this study may indicate. The interplay of other possible effects in addition to insufficient bleaching that would cause overestimation in both the luminescence-corrected and dose-corrected data include uncorrected changes in luminescence sensitivity, inadequate background assessment and extrapolation uncertainties. SAR protocols adapted to feldspars, although presently giving D_e underestimates (e.g. Wallinga et al., 2000a, b), may possibly be utilized in future studies to determine if concordance between quartz and feldspar can be improved. Due to the problems encountered early on in this work with K-feldspar OSL, further work concentrated solely on quartz SAR analyses.

Assessing all 146 quartz SAR measurements made on the 12 samples with reference to a recycling ratio threshold values of 0.9–1.1, indicates that the sensitivity correction fails ~32% of the time. This is slightly misleading because only 5 of the 12 samples contribute

to this figure. Of these five samples, the individual sample failure rate varies from $\sim 38\%$ to 87% and the mean value is $\sim 60\%$. However, the failure of the correction method only affected 3 of these 5 samples to a degree where confidence in the dating result was questioned (Table 3, footnote d). Interestingly, these three samples have highest D_e values (> 100 Gy) of the 12 samples investigated, and the failure of sensitivity correction may therefore possibly be dose-dependent. Only one of the samples (UCR_062) had consistently high (i.e. $> 5\%$) thermal transfer.

The histogram in Fig. 6b shows a skewed distribution of D_e values inferring the sample contains a mixture of bleached and unbleached quartz grains. Conversely, the same histogram also indicates that a cluster of D_e values is present at lowest doses between 25 and 35 Gy. This behaviour is shown in the majority of samples measured. Although, in this study, individual SAR measurements were carried out on several hundred quartz grains per disc and due to hardware constraints the number of repeat measurements within available machine time was limited, we believe it is appropriate to make an analogy with the findings of Olley et al. (1998, 1999). They measured ‘small’ aliquots and single grains from fluvial sediments, and concluded that the best estimate of the true burial dose is the lowest measured dose population. Therefore, we suggest that the low-dose cluster evident in the example in Fig. 6b represents the distribution of D_e values for the true burial dose of the samples. For comparison, the histogram in Fig. 6a indicates tightly grouped D_e values and therefore, in this example, all measurements are used to determine the mean D_e .

We rate confidence in the quartz SAR results according to the number of repeat measurements n (Table 3), identified from histograms of D_e distribution (e.g. Fig. 6), used to calculate the mean D_e (Table 3), after removal of results which move the mean recycling ratio outside the 0.9–1.1 threshold range. In this way, we place the highest confidence in the quartz SAR results from samples UCR_055 and UCR_060. This is confirmed by virtue of their excellent agreement with feldspar-SAAD (e.g. UCR_055; Figs. 4a and 5a). These samples are both from glaciolacustrine deposits and provide a maximum age and directly date the Ghulkin II Glacial Stage (t5) to 8.7 ± 0.8 and 12.0 ± 1.1 ka, respectively (locations A and E, Figs. 2A and 3A, and Figs. 2E and 3E).

We place UCR_059 and UCR_063 as the next most reliable results. UCR_059 is also from a glaciolacustrine deposit and provides a minimum age for the Ghulkin II Glacial Stage (t5) of 18.0 ± 1.7 ka (location D, Figs. 2D and 3D). UCR_063 is from a glaciofluvial deposit and dates the Pasu I Glacial Stage (t7) to 8.4 ± 0.9 ka (location H, Figs. 2H and 3H). However, as we discuss below, the result for UCR_063 is very likely to be overestimated.

The next group of samples is UCR_056, UCR_057, UCR_061, UCR_062 and UCR_067. UCR_056 is a glaciofluvial sample and directly dates the glacial-maximum for the Ghulkin I Glacial Stage (t4) to an age of 18.4 ± 1.6 ka (location B, Figs. 2B and 3B); UCR_057 is from a glaciolacustrine deposit and provides a minimum age for the Batura Glacial Stage (t6) of 28.5 ± 2.7 ka (location C, Figs. 2C and 3C); UCR_061 is a glaciolacustrine sample and directly dates the glacial-maximum for the Batura Glacial Stage (t6) to an age of 7.8 ± 0.7 ka (location F, Figs. 2F and 3F); UCR_062 dates the Pasu I Glacial Stage to 4.3 ± 0.4 ka (location G, Figs. 2G and 3G), although this result must be treated with caution due to high thermal transfer; and, UCR_067 is from a glaciolacustrine deposit and directly dates the Ghulkin I Glacial Stage (t4) to 31.5 ± 3.0 ka (location K, Figs. 2K and 3K).

The final three samples with lowest number of repeats and lowest confidence are UCR_064, UCR_066 and UCR_070. UCR_064 is only based on a single measurement and provides a minimum age for the Batura Glacial Stage (t6) of 22.8 ± 3.6 ka (location I, Figs. 2I and 3I). For UCR_066, based on three repeats, it was not possible to determine unequivocally whether the moraine from which this sample was taken belonged to the Borit Jheel Glacial Stage (t3) or was part of the Pasu glacial catchment extending southwards along the diffuence col (Fig. 1) during the Ghulkin I Glacial Stage (t4). Therefore, UCR_066 dates either t3 or t4 to 31.6 ± 3.3 ka (location J, Figs. 2J and 3J). Finally, UCR_070 provides a minimum age for the Ghulkin I Glacial Stage (t4) of 44.4 ± 5.2 ka (location L, Figs. 2L and 3L).

7.2. Comparison of OSL with C-14, TL and CRN dates

The optical dates (UCR_063 and UCR_062) bracket the timing of the Pasu I Glacial Stage (t7) to between 8.4 ± 0.9 and 4.3 ± 0.4 ka. In contrast, Derbyshire et al. (1984) assigned an uncalibrated C-14 age range of 325 ± 60 and 830 ± 80 yr BP (Table 1). The timber and wood fragments on which the C-14 dates are based were sampled from a moraine associated with the Minapin glacier. This glacier is located in the Hunza valley ~ 60 km downstream from Pasu, a few km south of the Hunza River and to the east of Rakaposhi (Fig. 1A). It is difficult to ascertain how well the Minapin moraines represent the Pasu I Stage, but it is clear from Fig. 1 that the lateral t7 moraines parallel the present glacial margins of the Batura, Pasu and Ghulkin glaciers. This therefore suggests a relatively young age for this Stage indicating that the optical dates are overestimated. Furthermore, as discussed above, the optical date for UCR_062 must be treated with caution due to high thermal transfer levels. Measurement of a large number of small aliquots or single grains of quartz from

UCR_062 and UCR_063 may provide lowest measured dose populations that represent true burial doses for these samples (cf. Olley et al., 1998, 1999; Spencer et al., 2003). The chronology of the Pasu I Glacial Stage was not investigated using CRN dating techniques.

For the Batura Glacial Stage (t6) the optical dates (UCR_057, UCR_064 and UCR_061) provide minimum ages for the Stage of 22.8 ± 3.6 and 28.5 ± 2.7 ka and give a glacial-maximum age of 7.8 ± 0.7 ka. In comparison, CRN dating gives an age range of 9.0–10.8 ka. The OSL and CRN results give relatively concordant dates for the maximum extent of the Stage. Fig. 7 indicates that UCR_057 (28.5 ± 2.7 ka) is more likely dating a depositional event associated with the Ghulkin I Glacial Stage (t4). The same could be true of UCR_064 (22.8 ± 3.6 ka) but since this result is only from one measurement (14 out of 15 measurements were rejected; see Table 3), and we therefore have no assessment of the form of D_e distribution, the date is unreliable and we can only presume that the sample should pre-date t6 on the basis of stratigraphy. No TL or C-14 dates were reported by Derbyshire et al. (1984) for the Batura Stage.

From Table 3 and Fig. 7, we see that the optical dates (UCR_059, UCR_060 and UCR_055) bracket the timing of the Ghulkin II Glacial Stage (t5) to between 18.0 ± 1.7 and 8.7 ± 0.8 ka, and indicate an age within the Stage of 12.0 ± 1.1 ka. In comparison, CRN dating gives an age range of 15.3–18.4 ka. Both OSL and CRN effectively give the same age for the beginning of the Stage, but OSL indicates the Stage lasted for a much longer time period of ~ 10 ka compared to ~ 3 ka. We would expect the correct CRN age range to be closer to the maximum age for the Stage from OSL (i.e. 8.7 ± 0.8 ka), or at least closer/younger than the OSL age within the Stage (12.0 ± 1.1 ka). The reason for this is that CRN techniques are effectively dating the time at which the glacier is beginning to retreat and depositing its final boulders onto the moraine ridges. It is difficult to explain this apparent discordance since it does not seem feasible that every boulder sampled has inherited CRNs; if inheritance was a factor, we would probably expect a greater range in CRN dates with youngest ages closer to ~ 11 – 12 ka. No TL or C-14 dates were reported by Derbyshire et al. (1984) for the Ghulkin II Stage.

The Ghulkin I Glacial Stage (t4) is bracketed by a maximum OSL age (UCR_070) of 44.4 ± 5.2 ka and a glacial-maximum OSL age (UCR_056) of 18.4 ± 1.6 ka, and directly dated (UCR_067) to 31.5 ± 3.0 ka within the Stage. In comparison CRN gives an age range of 21.8–25.7 ka. We have high confidence in the optical age (UCR_056) that dates the maximum extent of the glaciation, due to high internal consistency from replicated single-aliquot measurements, and this therefore suggests that the CRN data may contain an inherited component. Conversely, it is encouraging that the CRN dates are significantly younger than the OSL

dates from within and pre-dating t4, since, as discussed above, correct CRN data from glacial boulders on moraine ridges should record final stages of moraine development. Derbyshire et al. (1984) report a TL date of 47.0 ± 2.4 ka (Table 1), although no details of the dating methods were published so it is unclear if effects of insufficient bleaching were investigated. On the basis of the OSL and CRN chronology and the poorer bleaching of TL compared to OSL, it is likely that the TL date is an overestimate.

As discussed above, we are not certain whether UCR_066 was sampled from a moraine deposited during the Borit Jheel Glacial Stage (t3) or the Ghulkin I Glacial Stage (t4). Although this result is only based on three measurements it is more likely that the sample is dating the Ghulkin I Glacial Stage (t4) due to the good agreement between this result and UCR_067.

From Table 3 we see that the absolute uncertainty of the OSL ages is ~ 9 – 12% at 1-sigma (16% for the single value of UCR_064). This compares with a value of ~ 15 – 20% for cosmogenic data (Finkel, pers. comm.), which is principally due to the uncertainty in CRN production rates, although toppling, weathering, inheritance and exhumation are all potential contributory factors (e.g. Owen et al., 2002a).

7.3. Verification of paleoclimatic interpretations

The OSL result that dates the glacial-maximum age of the Batura Glacial Stage (t6) (UCR_061; 7.8 ± 0.7 ka) represents an early Holocene advance. Owen et al. (2002a) draw the same conclusion from their CRN age range of 9.0–10.8 ka. The OSL result that directly dates the Ghulkin II Glacial Stage (t5) (UCR_060; 12.0 ± 1.1 ka) is right on the margin between MIS2 and MIS1 indicating a maximum Late Glacial age for t5, and possible indication of a Younger Dryas age. However, further measurements are required to test this since the Younger Dryas is so short (11.6–12.9 ka). Owen et al. (2002a) also assign a Late Glacial age for t5 although their range of CRN dates (15.3–18.4 ka) predate the Late Glacial Interstadial and they suggest possible correlation with Heinrich Event 1. The OSL result that dates the glacial-maximum age of the Ghulkin I Glacial Stage (t4) (UCR_056; 18.4 ± 1.6 ka) indicates a Last Glacial Maximum age for this Stage. Owen et al. (2002a) also suggest a Last Glacial Maximum age for t4, but again the CRN age range is older at 21.8–25.7 ka and they indicate a possible correlation with Heinrich Event 2.

In each Stage discussed above, we would expect the OSL and CRN dates to have closer concordance. Although we do not have multiple optical ages from the same sampling site, the three OSL dates (UCR_061, UCR_060 and UCR_056) have high internal consistency from replicated single-aliquot measurements. Further-

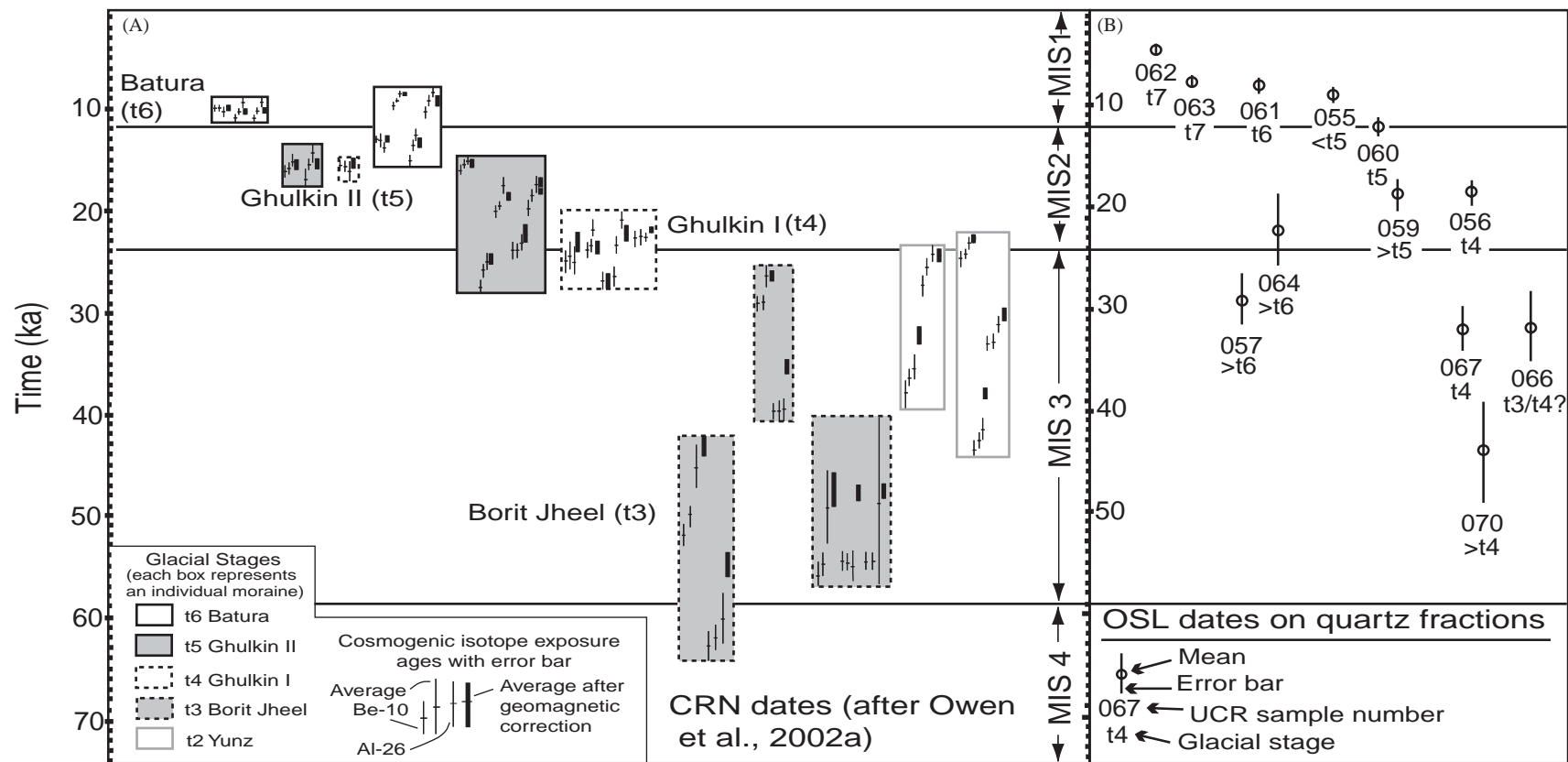


Fig. 7. (A) CRN ages for moraines in the Hunza valley (Owen et al., 2002a). Each box encloses samples from the same moraine. The horizontal lines represent the boundaries of the marine oxygen isotope stages (MISs). (B) OSL dates on 90–125 μm quartz fractions extracted from sediment matrices.

more, because of the well-documented problems of insufficiently bleached luminescence signals in sediments from high-energy mountain environments, we would expect the optical dates to be overestimated rather than underestimated. For the CRN data, the careful sampling strategy employed by Owen et al. (2002a) ensured that processes that would cause underestimation of the CRN age of boulders such as toppling, weathering and exhumation are less likely to be present. There is, therefore, a possible indication of inherited components in the CRN data. However, in terms of paleoclimate, the OSL results are broadly interpreted in the same way as the CRN data in comparison with marine oxygen isotopic stages.

8. Conclusion

Twelve samples from Late Quaternary glaciogenic sediments from the upper Hunza valley in northern Pakistan were studied using luminescence dating methods. Quartz and K-feldspar minerals were extracted from the sediments and dated using OSL single-aliquot techniques. Analysis of SAAD growth curves from initial K-feldspar measurements indicated early onset of signal saturation in the majority of samples suggesting inadequate bleaching of remnant geological luminescence at deposition. Further work concentrated on replicated quartz measurements using the SAR method. In general the sensitivity correction technique employed in the quartz-SAR method worked satisfactorily; confidence in the dating result was only considered to be poor for 3 out of the 12 samples studied due to failure of the correction method. Thermal transfer was only a significant factor for 1 of the 12 samples. We used histogram plots to examine the D_e distribution in our quartz data. The majority of histograms indicated low-dose populations that we believe represent the distribution of D_e values for the true burial dose of the samples. This is shown to be a good assumption in most cases by virtue of concordance with K-feldspar for two samples, concordance between OSL and CRN in terms of paleoclimate interpretations and stratigraphic consistency throughout.

Acknowledgements

Bob Finkel (Lawrence Livermore National Laboratory, California) and Marc Caffee (Lawrence Livermore National Laboratory, California and Purdue University, Indiana) for their excellent companionship and field assistance in northern Pakistan. Andrew Murray (Risø) for very useful discussions. Kimberly Le for laboratory assistance at UCR. The University of California for

providing financial support to undertake fieldwork in the Hunza region and for laboratory analyses.

References

- Adamiec, G., Aitken, M., 1998. Dose-rate conversion factors: update. *Ancient TL* 16, 37–50.
- Aitken, M.J., 1998. *An Introduction to Optical Dating*. Oxford University Press, Oxford.
- Anderson, S.P., Drever, J.I., Humphrey, N.F., 1997. Chemical weathering in glacial environments. *Geology* 25, 399–402.
- Bortolot, V.J., 1997. Improved OSL excitation with fiberoptics and focused lamps. *Radiation Measurements* 27, 101–106.
- Derbyshire, E., Li Jijun, Perrott, F.A., Shuying, Xu., Waters, R.S., 1984. Quaternary glacial history of the Hunza Valley, Karakoram Mountains, Pakistan. In: Miller, K. (Ed.), *International Karakoram Project*. Cambridge, Cambridge University Press, pp. 456–495.
- Duller, G.A.T., 1991. Equivalent dose determination using single aliquots. *Nuclear Tracks and Radiation Measurements* 18, 371–378.
- Duller, G.A.T., 1994. Luminescence dating of sediments using single aliquots: New procedures. *Quaternary Geochronology (Quaternary Science Reviews)* 13, 149–156.
- Eyles, N., Eyles, C., Miall, A.D., 1983. Lithofacies types and vertical profile models; an alternative approach to the description and environmental interpretation of glacial diamict and diamictite sequences. *Sedimentology* 30, 393–410.
- Finkel, R.C., Owen, L.A., Barnard, P.L., Caffee, M.W., 2003. Beryllium-10 dating of Mount Everest moraines indicates a strong monsoonal influence and glacial synchronicity throughout the Himalaya. *Geology* 31, 561–564.
- Li, S.-H., 1991. Removal of the thermally unstable signal in optical dating. *Ancient TL* 9, 26–29.
- Mejdahl, V., 1979. Thermoluminescence dating: beta attenuation in quartz grains. *Archaeometry* 21, 61–73.
- Mejdahl, V., 1988. Long-term stability of the TL signal in alkali feldspars. *Quaternary Science Reviews* 7, 357–360.
- Murray, A.S., Wintle, A.G., 2000. Luminescence dating of quartz using an improved single-aliquot regenerative-dose protocol. *Radiation Measurements* 32, 57–73.
- Olley, J.M., Murray, A., Roberts, R.G., 1996. The effects of disequilibria in the uranium and thorium decay chains on burial dose rates in fluvial sediments. *Quaternary Science Reviews (Quaternary Geochronology)* 15, 751–760.
- Olley, J.M., Caitcheon, G.G., Murray, A.S., 1998. The distribution of apparent dose as determined by optically stimulated luminescence in small aliquots of fluvial quartz: implications for dating young sediments. *Quaternary Science Reviews (Quaternary Geochronology)* 17, 1033–1040.
- Olley, J.M., Caitcheon, G.G., Roberts, R.G., 1999. The origin of dose distributions in fluvial sediments, and the prospect of dating single grains from fluvial deposits using optically stimulated luminescence. *Radiation Measurements* 30, 207–217.
- Owen, L.A., 1993. Glacial and non-glacial diamictons in the Karakoram Mountains. In: Croots, D., Warren, W. (Eds.), *The Deposition and Deformation of Tills*. A.A. Balkema, Rotterdam, pp. 9–29.
- Owen, L.A., 1996. Quaternary lacustrine deposits in a high energy semi-arid mountain environment, Karakoram Mountains, northern Pakistan. *Journal of Quaternary Science* 11, 461–483.
- Owen, L.A., Fort, M., Derbyshire, E., 1998. The Quaternary glacial history of the Himalaya. *Quaternary Proceedings* 6, 91–120.
- Owen, L.A., Gualtieri, L., Finkel, R.C., Caffee, M.W., Benn, D.I., Sharma, M.C., 2001. Cosmogenic radionuclide dating of glacial landforms in the Lahul Himalaya, northern India: constraining the

- timing of Late Quaternary glaciation. *Journal of Quaternary Science* 16, 555–563.
- Owen, L.A., Finkel, R.C., Caffee, M.W., Gualtieri, L., 2002a. Timing of multiple glaciations during the Late Quaternary in the Hunza Valley, Karakoram Mountains, northern Pakistan: defined by cosmogenic radionuclide dating of moraines. *Geological Society of America Bulletin* 114, 593–604.
- Owen, L.A., Kamp Jr., U., Spencer, J.Q., Haserodt, K., 2002b. Timing and style of Late Quaternary glaciation in the eastern Hindu Kush, Chitral, northern Pakistan: a review and revision of the glacial chronology based on new optically stimulated luminescence dating. *Quaternary International* 97–98, 41–55.
- Phillips, W.M., Sloan, V.F., Shroder, J.F., Sharma, P., Clarke, M.L., Rendell, H.M., 2000. Asynchronous glaciation at Nanga Parbat, northwestern Himalaya Mountains, Pakistan. *Geology* 28, 431–434.
- Prescott, J.R., Hutton, J.T., 1994. Cosmic ray contributions to dose rates for luminescence and ESR dating: large depths and long-term time variations. *Radiation Measurements* 23, 497–500.
- Preusser, F., 1999. Bleaching characteristics of some optically stimulated luminescence signals. *Ancient TL* 17, 11–14.
- Rhodes, E.J., 2000. Observations of thermal transfer OSL signals in glacial quartz. *Radiation Measurements* 32, 595–602.
- Richards, B.W.M., 2000. Luminescence dating of Quaternary sediments in the Himalaya and High Asia: a practical guide to its use and limitations for constraining the timing of glaciation. *Quaternary International* 65–66, 49–61.
- Richards, B.W., Owen, L.A., Rhodes, E.J., 2000a. Timing of Late Quaternary glaciations in the Himalayas of northern Pakistan. *Journal of Quaternary Science* 15, 283–297.
- Richards, B.W., Benn, D.I., Owen, L.A., Rhodes, E.J., Spencer, J.Q., 2000b. Timing of Late Quaternary glaciations south of Mount Everest in the Khumbu Himal, Nepal. *Geological Society of America Bulletin* 112, 1621–1632.
- Spencer, J.Q., Sanderson, D.C.W., Deckers, K., Sommerville, A.A., 2003. Assessing mixed dose distributions in young sediments identified using small aliquots and a simple two-step SAR procedure: the *F*-statistic as a diagnostic tool. *Radiation Measurements* 37, 425–431.
- Spooner, N.A., Questiaux, D.G., Aitken, M.J., 2000. The use of sodium lamps for low-intensity laboratory safelighting for optical dating. *Ancient TL* 18, 45–49.
- Wallinga, J., Murray, A., Duller, G., 2000a. Underestimation of equivalent dose in single-aliquot optical dating of feldspars caused by preheating. *Radiation Measurements* 32, 691–695.
- Wallinga, J., Murray, A., Wintle, A., 2000b. The single-aliquot regenerative-dose (SAR) protocol applied to coarse-grain feldspar. *Radiation Measurements* 32, 529–533.
- von Wissman, H., 1959. Die heutige Vergletscherung und Schneegrenze im Hochasien, mit Hinweisen auf die Vergletscherung der Letzen Eiszeit. *Akademie Wissenschaften und der Literatur, Mainz, Abhandlungen der Marh.—Naturwissenschaftlichen Klasse, Jahrg 14*, 1105–1407.